JOURNAL OF THERMOPHYSICS AND HEAT TRANSFER
Vol. 18, No. 1, January–March 2004

Kinetic Model for Simulation of Aerosol Droplets in High-Temperature Environments

Craig M. Benson*
George Washington University, Washington, D.C. 20052
Deborah A. Levin,† Jiaqiang Zhong,‡ and Sergey F. Gimelshein§
Pennsylvania State University, University Park, Pennsylvania 16802
and
Akbar Montaser¶
George Washington University, Washington, D.C. 20052

A kinetic flow model to determine the behavior of aerosol droplets injected into a high-temperature gas environment is presented. Droplet heating, desolvation, coalescence, and transport are considered. The desolvation rate of droplets is calculated with a continuum heat transfer and a mass-loss model that uses the Fuks correction to account for kinetic effects. Droplet transport is modeled with the Cunningham slip flow correction factor applied to Stokes's law. The direct simulation Monte Carlo method is used to model droplet–droplet collisions, with the collision outcome determined with the use of the Ashgriz–Poo coalescence model. The developed computational tool is applied to the simulation of droplet evolution in a spatially uniform background gas and that of an argon inductively coupled plasma (ICP). We find that consideration of transitional regime effects reduces the desolvation rate and the droplet drag. In addition, the simulation shows that droplet coalescence leads to a significant increase in the penetration depth of the aerosol even into a high-temperature ICP environment.

Nomenclature

B = transfer number
C_D = drag coefficient
c_p = heat capacity at constant pressure
c_{rel} = relative collision velocity
D = diffusion coefficient
d = droplet diameter
d_m = molecular diameter
F = drag force
H = heat transfer coefficient
h = width of overlapping region of colliding droplets
Kn = Knudsen number
k = thermal conductivity
k_B = Boltzmann's constant
L = latent heat of vaporization
M = mass flux
m = mass
n = number density
p = pressure
Q = heat flux
Re = Reynolds number
T = temperature
v = relative velocity
We = Weber number
Y = mass fraction
α = accommodation coefficient
γ^* = adiabatic constant, 1.67
Δ = droplet size ratio
δ = thickness of limiting sphere
η = viscosity
λ = mean free path
μ = mean molecular spacing
ρ = density
σ = surface tension
χ = impact parameter

Subscripts

a = ambient gas
b = boiling
c = continuum
d = droplet
e = evaporation
g = gas surrounding the droplet
M = mass
r = reference
s = droplet surface
T = thermal
v = vapor
δ = within limiting sphere
ω = constant parameter for heat transfer calculation
∞ = environment far from droplet

Received 17 March 2003; revision received 13 June 2003; accepted for publication 19 June 2003.

*Graduate Student, Department of Chemistry; currently Postdoctoral Fellow, Remote Sensing Division, Naval Research Laboratory, Washington, DC 20375.
†Associate Professor, Department of Aerospace Engineering. Senior Member AIAA.
‡Graduate Student, Department of Aerospace Engineering. Member AIAA.
§Senior Research Associate, Department of Aerospace Engineering. Member AIAA.
¶Professor, Department of Chemistry.

I. Introduction

THE behavior of droplets in a spray is of interest in diverse fields such as analytical chemistry, investigation of space plumes, and the design of internal combustion engines. For example, sample introduction in inductively coupled plasma (ICP) spectrometry typically utilizes a fine spray of dilute aqueous analyte. Several processes occur as a spray propagates through an environment, such as droplet heating or cooling due to gas–droplet temperature difference, evaporation, and coalescence due to droplet–droplet collisions, and droplet transport through the gaseous medium. Each of these processes, as well as any effects due to an increase in the droplet

Knudsen number, must be represented in a comprehensive spray model. Thus, a computer simulation is needed to address these issues. The model developed in this work assumes that the droplets do not change the background gas flow properties.

A key parameter in the modeling of aerosol droplets is the local droplet Knudsen number, given by

$$Kn = \lambda_a / d \tag{1}$$

where λ_a is the mean free path of the ambient gas, argon, and d is the diameter of the droplet. The Knudsen number increases as the droplet evaporates or as the temperature of the gaseous medium at a specific pressure increases, leading to a larger mean free path. In this case, corrections are necessary to the continuum heat and mass transfer equations, as well as the drag force exerted by external gas flows. The necessary modifications are discussed later and implemented in the model.

Several models have been developed to determine evaporation and transport of droplets in the high-temperature environments characteristic of spectroscopic devices.[1,2] However, our approach is unique due to the inclusion of two important effects.[3–6] First, the change to the desolvation rate and the drag coefficient due to the droplet Knudsen number is included, allowing the model to be extended to higher temperatures. Second, the coalescence of liquid drops subsequent to a collision is considered and modeled at a kinetic level. As discussed in the following sections, these effects greatly influence the spatial distribution of droplets in a high-temperature, two-phase flow.

The purpose of this paper is to present the details of the two-phase flow modeling and computational tool that we have developed. The goal of the effort has been to create a model suitable for describing the flow behavior of an entire system of gas and droplets, not just the gas flow about a single droplet. To provide a flow methodology sufficiently general to incorporate kinetic effects, a direct simulation Monte Carlo (DSMC) approach is used. The DSMC technique has been applied successfully to model rarefied gas flows[7]; however, in this application it is used to simulate the droplet behavior. Because this application deviates significantly from the usual practice, the range of applicability is examined in the following section. A droplet transport method must be selected because the gas and droplets are not stagnant. In Sec. III we consider a statistical and a deterministic approach, the selection of a particle drag model, and the validation of the proposed droplet transport model. We then discuss the destruction and creation processes of water droplets in a high-temperature gas. Droplet loss, discussed in Sec. IV, arises primarily due to the evaporation of the solvent. This is accomplished via the two separate but closely related processes of heat transfer and mass loss. Energy (heat) transfer from the background gas to the droplet leads to droplet heating. A continuum model is implemented in the DSMC simulations to calculate heat transfer. A model for the second of the evaporation processes, mass loss or desolvation, that accounts for kinetic effects is presented. Droplet loss in a high-temperature gas can be reduced through the process of coalescence as discussed in Sec. V. Finally, in Sec. VI we present modeling predictions of particle spatial distributions for initially constant-sized droplets in a background gas at a constant temperature, as well as predictions of a direct-injection high-efficiency nebulizer (DIHEN)[8] particle spray distribution in an argon ICP. Atmospheric-pressure argon ICP is a useful desolvation–vaporization–atomization–excitation–ionization source for atomic emission and mass spectrometries.[9,10] The sample solution is most commonly introduced into an ICP via a dilute aqueous spray and, in terms of the device efficiency, the droplet desolvation is the most important process. Numerical modeling can lead to a better understanding of the amount of detectable analyte in the nebulizer spray and also assist in nebulizer (and spray chamber) design.

II. Justification for the Use of DSMC

The motion and collisions of droplets are calculated with the DSMC method, a kinetic approach to the modeling of rarefied gas flows[7] that has also been successfully applied to modeling of flows in the near-continuum regime. The numerical scope of this research, however, differs from conventional applications of the DSMC method. The DSMC method is chosen because droplets exhibit particle behavior. It also offers accurate solutions for the spatially nonuniform master Leontovich equation for the N-particle distribution function in multidimensional flows. Under the conditions of molecular chaos, the Boltzmann equation may be derived[11] from the master kinetic equation for an N-particle system. The DSMC method may therefore be regarded as a statistical method for solving the Boltzmann equation.

The use of the DSMC method to model rarefied and even continuum flows is motivated by the validity of the Boltzmann equation for gas pressures up to several atmospheres. However, its applicability to the simulation of collisions and transport of micron-sized particles must be substantiated separately. The validity of the Boltzmann equation is related to the main assumptions that are made in the derivation. The principal restrictions are the requirement of a dilute gas/binary collisions and the molecular chaos hypothesis.

The assumption of a dilute gas implies[7] that only a very small proportion of space is occupied by the particles, and each particle for the most part of its trajectory is moving outside the range of influence of other particles. The first condition means that

$$d \ll \mu \tag{2}$$

where d is the particle diameter and μ is the mean spacing between particles related to the gas density n as

$$\mu = 1/n^{\frac{1}{3}}$$

When collisions between only two particles are the dominant process, the second condition characterizes the binary collision regime. In terms of collision times, the binary collision/dilute particle assumption maybe written as

$$t_d \ll t_c \tag{3}$$

where t_d is the mean duration of a collision, and t_c the mean collision time, which is, by definition, the mean time between the successive collisions suffered by any specific particle.

There are two possible collision processes that must be considered for the aerosol model in terms of the dilute particle conditions (2) and (3). The first type is related to the collisions between water droplets and background argon atoms, and the second is for the droplet–droplet collisions. Argon–argon particle collisions are not modeled because argon is assumed to be a background gas whose velocities do not change.

For argon–droplet collisions, the diameter of an argon atom is negligibly small compared to that of a droplet. Therefore, the relevant value for d is that of the droplet diameter. For a droplet number density[8] on the order of or less than 4×10^{13} droplets/m^3, the droplet diameter should be much less than the interdroplet spacing of $\mu = 30$ μm to satisfy Eq. (2).

Let us examine now the validity of the binary collision assumption for argon–droplet collisions. The collision duration may be evaluated roughly as the ratio of the argon diameter to the average relative collision velocity c_{rel} between argon and droplets:

$$t_d = d_{\text{argon}} / c_{\text{rel}} \approx 10^{-12}\ s$$

The mean collision time for a single 10-μm droplet surrounded by argon at 1 atm may be calculated using a hard sphere approximation,

$$t_c = 1/\pi d^2 n c_{\text{rel}} \approx 10^{-17}\ s \tag{4}$$

where d in this case is the average droplet–argon diameter, $(d_{\text{droplet}} + d_{\text{argon}})/2$ for a relative collisional velocity c_{rel} of 10 m/s. It is therefore clear that the mean collision time t_c is much smaller than the duration of a collision, and Eq. (3) for this type of interaction is not satisfied.

Similar to the preceding discussion of droplet–argon collisions, Eq. (2) is satisfied for droplet–droplet collisions. The binary collision requirement is also verified as follows. Our molecular dynamics calculations (to be discussed in Sec. V) also suggest that the mean collision time of two droplets is on the order of 10^{-7} s. The mean collision time may be evaluated using Eq. (4), and at the conditions

typical for the present work (10-μm droplets, the droplet number density of 4×10^{13} particles/m^3, and a relative droplet velocity of 10 m/s) it is about 10^{-5} s. This is much larger than the mean collision duration of 10^{-7} s, thus proving the validity of the binary collisions assumption, Eq. (3).

No correlation exists between the precollisional velocities of two colliding droplets because the successive collisions of a single droplet are widely separated relative to the droplet spacing;[12] that is, the molecular chaos hypothesis is fulfilled. In addition, the distribution function used in the Boltzmann equation is assumed not to vary significantly over a distance equal to the droplet diameter or in a time comparable to the duration of a collision. This assumption is valid considering the time and space scales of the aerosol flow. (The droplet diameter is on the order of microns, and the flow changes on the scale of millimeters.)

In sum, one can state that the Boltzmann equation (and therefore the DSMC method) is applicable to treat droplet–droplet collisions, but does not rigorously satisfy the argon–droplet collisional criteria of Eq. (3). The error in using Eq. (3) is not known a priori and will be discussed in the next section. The statistical modeling in low-density environments (SMILE) computational tool,[13] based on the DSMC method, is used for all simulations and is extended to simulate droplet behavior. Several features (such as species and spatial weights and different grids for collisions and sampling of macroparameters) of the code improve the accuracy and efficiency of the simulation.[13]

III. Transport Process

The droplet transport process can strongly influence the droplet heat and mass transfer rates due to background gas gradients in temperatures and velocities. Droplet spatial and velocity distributions in the flowfield will depend on droplet size, droplet–background-gas relative velocity, and the temperature-sensitive coefficient of viscosity of the background gas. In Sec. VI, where results of the flow modeling are discussed, it will be seen that droplet distributions may be different due to these three properties with regions of droplets accumulation or spreading observed. For these reasons, it is important to establish the accuracy of the droplet transport model and its region of applicability for the flow conditions under consideration. First, we consider the trajectory modeling of 10-μm-sized droplets injected into a background gas of argon at a constant temperature of 2000 K and 1 atm pressure, moving with only an axial velocity for an axisymmetric geometry. Note that the properties of the background argon atoms, such as position and velocity, do not change in the simulation. Although this is a highly simplified flow condition we can determine the accuracy of the proposed transport model with an analytic result. We then use single-sphere DSMC calculations to choose the best model for the drag force of micron-sized droplets in the two-phase flow.

A. Comparison of Statistical and Deterministic Transport Methods

To simulate the droplet transport, we consider a model based on the DSMC procedure, denoted as a kinetic model, and a deterministic model based on Newton's equation of motion of the droplet. In the kinetic method, the DSMC technique is used to calculate the cell-averaged forces on the droplet due to argon collisions. Because the aerosol droplets are injected into a 1-atm background gas, the collisions between background atoms and droplets do not rigorously satisfy the rarefied gas assumption, as discussed in Sec. II. We do not know a priori how large the error may be in using a kinetic model; however, it can be estimated by comparison of the DSMC solution with the simple, analytic (Newtonian) result.

The DSMC calculation was performed using a computational domain of 0.03×0.004 m^2 with 300×40 cells. With the use of both radial weighting factors and a species weighting factor for the droplet particles, about 2,225,580 argon gas particles and 15,000 droplets were modeled to simulate the transport process. The radial weighting factors for axisymmetric flows are discussed in Ref. 11. The species weights imply the use of different real-to-simulated molecule ratios, F_{num}, for different gas species. In the calculations discussed in this subsection, species weights were used in the statistical transport model due to the large difference between the argon and droplet densities. The number density of argon is on the order of 3×10^{24} particle/m^3 and the number density of water droplets at the inflow boundary is 4.12×10^{13} particle/m^3. Values of 0.6×10^{12} and 0.6×10^{1} were therefore taken for the argon and droplet F_{num}, respectively. To decrease the number of argon–droplet collisions and increase the efficiency of these collisions (i.e., momentum transfer in a single collision), collision weights were also used in the DSMC transport calculations. The use of these weights implies the application of a scale factor to increase the momentum transfer per collision and proportionally decrease the collision frequency between argon and droplets. Different collision weights were assumed in these calculations depending on the size of the droplets, with the general rule of having a virtual argon mass of about 0.1% of the droplet mass.[3] Several different values for the collision weights were tried and it was found that the results remained the same, while the computational efficiency improved significantly. Monosized droplets with 10-μm diameter have an average initial velocity of 10 m/s in the axial direction and the background argon atoms have a fixed average velocity of 500 m/s, a pressure of 1 atm, and a temperature of 2000 K. A time step of 1×10^{-7} s was used to ensure that the droplet displacement per time step was less than one cell size. Results were sampled at the 5000th time step. Solutions were also obtained with a finer grid and larger numbers of samples to ensure that the result were accurate and grid independent.

Figure 1 shows a comparison of the kinetic solution compared with a simple differential equation of the droplet motion. Two analytic droplet model calculations were performed for the latter case.

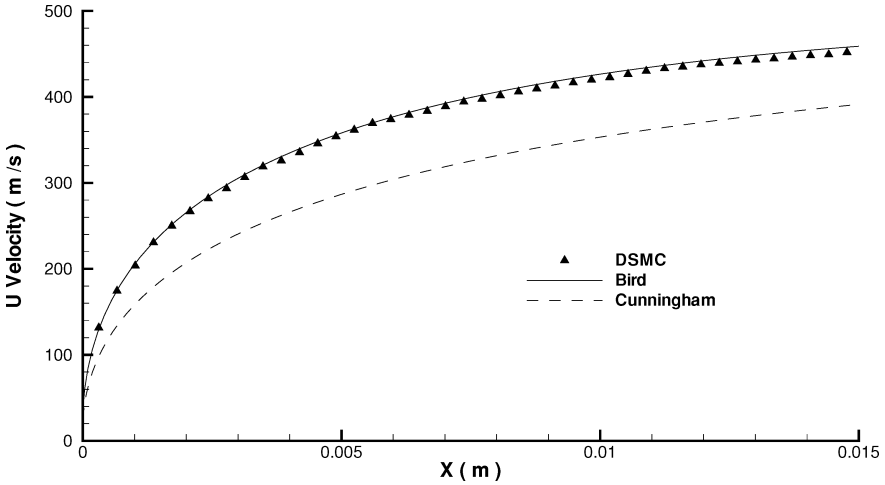

Fig. 1 Comparison of DSMC particle transport calculations with analytic expressions (curves labeled Bird and Cunningham) for 10-μm droplets into a background gas of 1 atm, temperature of 2000 K, and a fixed, average velocity of 500 m/s.

In the first one, the drag force is obtained by integrating the momentum flux given by Bird[7] assuming diffuse reflection, and in the second calculation a coefficient of drag given by Cunningham is used.[14] When the Cunningham drag coefficient is used, the droplet travels 9.52 cm to reach 90% of its final velocity. In contrast to the analytic solutions, the kinetic DSMC solution is obtained by averaging the droplet velocity in each cell. The expression for the drag coefficient derived from the momentum flux given by Bird (Ref. 7, p. 82) corresponds to free-molecular conditions, whereas that of Cunningham[14] corresponds to that of slip flow. We will show that the latter case is closer to the conditions of interest. It can be seen from the figure that the kinetic model is in good agreement with the free-molecular analytic result, but in poor agreement with the analytic result that uses the correct coefficient of drag (of Cunningham). This discrepancy may be understood as follows. The DSMC procedure models a collision between gas and droplet particles in a cell assuming that collisions are independent of other collisions and that there are no gradients in the cell. Hence, the forces on the droplet calculated with the kinetic DSMC model and the free-molecular analytic model should be the same. The disagreement with the analytic slip-flow drag coefficient is due to gradients of background-gas properties in the vicinity of the droplet that are being ignored in these DSMC calculations. Decreasing cell size in the vicinity of each droplet to resolve these gradients in a full simulation would be impractical. We can see from Fig. 1 that the error in using a kinetic model is unacceptably too large. Hence, the droplets will be transported in a deterministic manner using a selected coefficient of drag, to be discussed.

B. Determination of the Coefficient of Drag by Single-Sphere Calculations

As mentioned earlier, in the full simulation of the two-phase flow system it is not computationally feasible to use a grid that permits the modeling of the flow about each individual, moving droplet. For this reason, a phenomenological model that captures the important physical properties as a function of droplet Reynolds and Knudsen numbers is sought. DSMC simulations of the gas flow past a single sphere were performed to determine the most accurate analytic expression for the drag force in the slip-flow regime. The single-sphere DSMC simulations consist of a stationary, 1-μm-diam diffusely reflecting sphere in the center of an 8×8 μm^2 axisymmetric domain with a 5 m/s gas flow (U) of atomic mass, 14 g/mole. The droplet surface and the gas temperatures were assumed to be 300 K. The gas number density was varied to study Knudsen numbers of 0.1, 0.3, and 0.5. The force exerted against the sphere due to the gas flow was calculated to determine the drag coefficient. Each simulation was performed for 350,000 time steps, where each time step was 8×10^{-11} s, and used approximately 3×10^6 gas particles. The solutions were determined to be converged with respect to the size of the computational domain by comparison with a larger one of 24×24 μm^2. The very low velocities of the three flow cases considered (Table 1) make it difficult to obtain solutions of the highest accuracy.

To assess the accuracy of the DSMC calculations, a single-sphere DSMC calculation at $Kn = 10,000$ for $Re = 1.2 \times 10^{-6}$ was compared with an analytic expression[15] for the coefficient of drag in the free-molecular regime. Using the total drag coefficient for a diffuse reflecting sphere of Ref. 15 for a speed ratio $s = 8.376 \times 10^{-3}$, where

$$s = U/\sqrt{2RT}$$

Table 1 Predicted drag coefficients based on the single-sphere DSMC simulations and Stokes law with the Cunningham slip-flow correction[19]

Kn	Re	DSMC simulation	Cunningham correction
0.1	0.1213	184.2	158.0
0.3	0.0404	314.5	331.0
0.5	0.02426	406.4	414.0

the coefficient of drag in the free-molecular limit is 500.3. The corresponding DSMC single-sphere calculation gives a value within 0.8% of this value, an indication of the minimum error in the DSMC single-sphere calculations. The actual error in the transitional Knudsen number DSMC calculations, based on a value of three times the root-mean-square deviation of the computed drag coefficient, is 6% for a Knudsen number of 0.1 and 4% for the two other Knudsen number cases. The DSMC calculations are therefore sufficiently accurate for the selection of a semi-empirical drag model.

The drag coefficients predicted by DSMC and other methods[14–18] are presented in Fig. 2 and Table 1. For the relatively low $Kn = 0.1$ case (Fig. 2a), the deviation of the coefficient of drag among the six techniques is small and in this case the Stokes model best agrees with the DSMC calculation. Figures 2b and 2c show that for the more rarefied flows ($Kn = 0.3$ and 0.5), the difference between the slip-flow correction models is increased. Because the goal is to choose a phenomenological model that can be used in the full spray simulation, we do not expect perfect agreement between exact (DSMC) and a single semi-empirical model. The DSMC results (Figs. 2b and 2c and Table 1) indicate that the Cunningham correction best predicts the drag force on a sphere for the range of conditions in the two-phase flows considered here. Using the slip-flow correction suggested by Cunningham,[14,19] the applicability of Stokes's law can be extended and is expressed as follows:

$$F = \frac{3\pi \eta_a v d}{1 + (\lambda_a/d)\{2.514 + 0.800 \exp[-0.55(d/\lambda_a)]\}} \tag{5}$$

At low Knudsen numbers, the denominator approaches 1, thus restoring the original form of Stokes's law, which is accurate in the continuum gas limit.

IV. Heat and Mass Transfer Process

The energy transfer from a high-temperature environment to the droplet is proportional to the difference between the environment temperature T_a and the surface temperature of the droplet, T_s.[20,21] Whereas this transfer causes a steady increase in T_s, water vapor lost through desolvation (mass transfer) can fully or partially counteract droplet heating due to evaporative cooling.[22] Energy transfer to the droplet is given by

$$Q = \pi d H (T_\infty - T_s) \tag{6}$$

where Q is the heat flux and H is the heat transfer coefficient.

Evaporative cooling is proportional to the surface area of the droplet, or the amount of water vapor lost via evaporation:

$$Q_e = 2\pi d (k_g/c_{p,g}) L \, \ell n(1 + B) \tag{7}$$

where k_g is the thermal conductivity of the gas surrounding the droplet, c_p is the heat capacity, L is the latent heat of vaporization, and B is the transfer number. The heat gain [Eq. (6)] is proportional to the difference in the gas and droplet temperatures, unlike heat loss [Eq. (7)]. Therefore, the heat transfer rate decreases with increasing droplet temperature. The droplet temperature reaches a steady-state value (the wet-bulb temperature) lower than the boiling temperature of water T_b.

The mass transfer is calculated concurrently with droplet heating. Again, the mass flux of the droplet is described by a continuum method.[20,21]:

$$M = 2\pi d (k/c_p)_g \, \ell n(1 + B) \tag{8}$$

where B is either the mass transfer number B_M or the heat transfer number B_T:

$$B_M = Y_{v,s}/(1 - Y_{v,s}) \tag{9}$$

$$B_T = c_{p,g}(T_\infty - T_s)/L \tag{10}$$

The mass fraction of vapor at the droplet surface, $Y_{v,s}$, is given by

$$Y_{v,s} = [1 + (p_\infty/p_{v,s} - 1)(m_a/m_v)]^{-1} \tag{11}$$

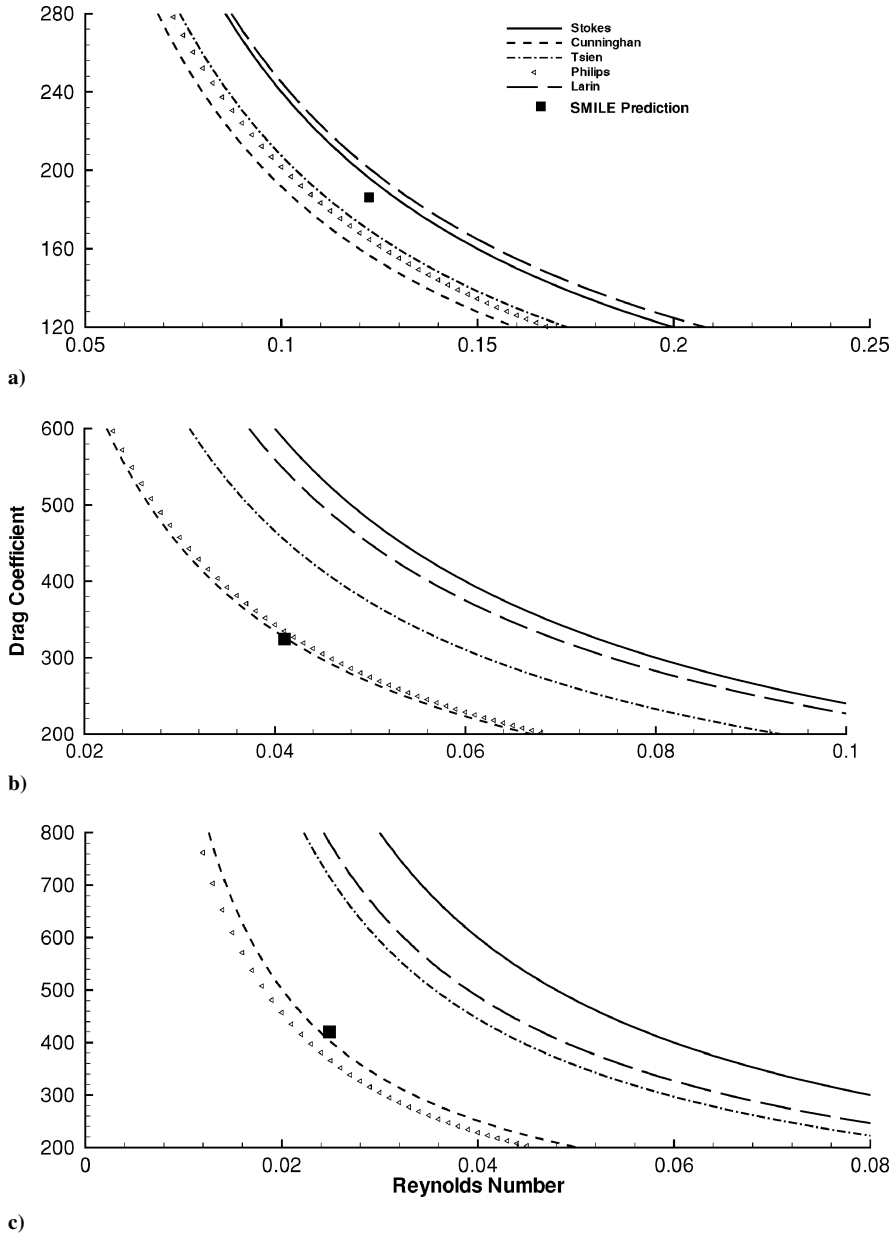

Fig. 2 Drag coefficient comparisons as a function of Reynolds number, calculated using different slip-flow correction models and the DSMC technique: *Kn* = a) 0.1, b) 0.3, and c) 0.5.

The Clausius–Clapeyron equation is used to obtain $p_{v,s}$ in Eq. (11).[23] During the heating period, evaporation is mass transfer limited, necessitating the use of B_M in Eq. (8). As the droplet approaches its boiling point, the value of B_M surpasses that of B_T, making the evaporation heat transfer limited and necessitating use of the latter parameter instead.[21] Properties of the gas surrounding the droplet (such as $c_{p,g}$ and k_g) are calculated at a reference temperature and mass fraction given by the one-third rule[24,25]:

$$T_r = T_s + (T_\infty - T_s)/3 \tag{12}$$

$$Y_{v,r} = Y_{v,s} + (Y_{v,\infty} - Y_{v,s})/3 \tag{13}$$

The preceding analysis yields a droplet desolvation rate that follows the d^2 law,[21] which states that the square of the diameter of an evaporating particle is linear with time; that is, the mass loss is proportional to the surface area of the droplet.

The droplet mass transfer model requires a correction as the gas mean free path approaches the droplet diameter. The model of Young[26] was considered, but a serious limitation is the requirement of small temperature gradients from the gas to the droplet. Instead the corrected mass flux given in the work of Fuks[27,28] was used:

$$M = M_c[D/d\bar{v}_v\alpha + d/(d + 2\delta)]^{-1} \tag{14}$$

where M_c is the mass flux of the droplet under continuum conditions [Eq. (8)], $\bar{v}_v$ is the mean velocity of a vapor molecule escaping from the droplet surface, and D is the diffusion coefficient, given by

$$D = \tfrac{3}{8}\pi\bar{v}_v\lambda_a(1 + m_v/m_a) \tag{15}$$

Substitution of Eq. (15) into Eq. (14) shows that the correction is a function of the droplet Knudsen number,

$$M = M_c[(3\pi Kn/8\alpha)(1 + m_v/m_a) + d/(d + 2\delta)]^{-1} \tag{16}$$

where a collisionless boundary of thickness δ surrounding the droplet is defined in the work of Filippov and Rosner.[29] Figure 3 shows the magnitude of this correction due to Fuks[28] as a function of Kn for a droplet-to-gas temperature ratio, $T_\delta/T_g = 10$. The corrected mass transfer converges with the continuum solution (dashed line) at low values of Kn as expected. The mass flux correction is small in the limit of the continuum regime; however, as the

Knudsen number increases, this correction becomes increasingly important.

Using Eqs. (8–16), we can compare the continuum (solid) and corrected-continuum (dashed) evaporation models. Figure 4 illustrates the correlation between diameter and evaporation time of a droplet with an initial diameter of 10 μm in 3000 and 7000 K environments. Note that for both continuum and corrected-continuum models, evaporation is slow until the droplet has reached its wet-bulb temperature. In the continuum model, the d^2 law is obeyed when the droplet reaches its wet-bulb temperature. Figure 4 also illustrates the change in the d^2 curve when the mass flux correction (dashed line) is utilized. The deviation from the linear d^2 behavior is noticeable for a gas temperature of 3000 K and is even larger for 7000 K.

V. Coalescence Process

Droplet–droplet collisions lead to one of three outcomes: coalescence, stretching separation, or reflexive separation.[30–33] In stretching separation, the region of overlap between two colliding droplets is small; thus, the droplets initially merge and subsequently separate as the remaining body of the droplets move in opposite directions. In reflexive separation, strong internal flows that lead to separation are generated due to high velocities.

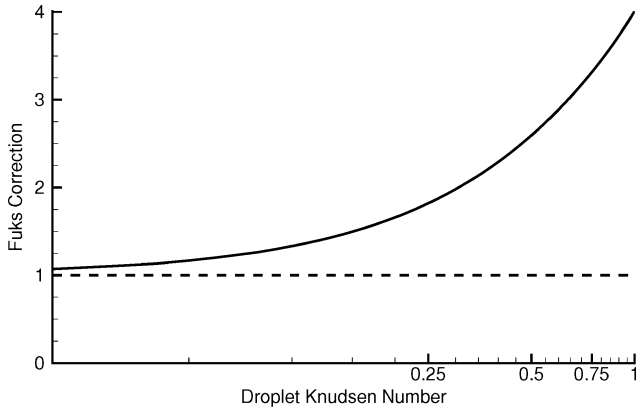

Fig. 3 Ratio of M_c/M indicating the importance of the Fuks correction as a function of droplet Kn. The dashed line indicates the uncorrected continuum solution.

The outcome of each collision is dictated by three factors: droplet size ratio (Δ, the diameter of the smaller droplet divided by that of the larger droplet), collisional Weber number (We, the ratio of the relative collisional kinetic energy to droplet surface energy), and impact parameter (χ, the normalized distance of closest approach of the centers of undisturbed droplet trajectories).[33] The Weber number is given by

$$We = \rho_d d_i v^2/\sigma_d \tag{17}$$

where d_i is the diameter of the smaller droplet, v is the droplet–droplet relative velocity, and σ_d is the liquid surface tension. A semi-empirical model, wherein analytic relationships are derived for the reflexive separation–coalescence and the stretching separation–coalescence boundaries as a function of Weber number and impact parameter, is discussed in Ref 33.

Figure 5 shows the predictions of Ashgriz and Poo[33] obtained for a droplet size ratio of 1.0. Note that stretching separation is primarily found at high impact parameters, whereas reflexive separation dominates at high Weber numbers and low impact parameters. In addition, the coalescence regime increases in size relative to the separation regimes as the droplet size ratio is decreased; that is, droplets are more likely to coalesce if their sizes are unequal.

Two possible limitations exist regarding the use of the Ashgriz and Poo[33] model. First, the model was derived and tested for droplets of millimeter size; thus, its applicability to smaller droplets is not directly known. Second, temperature dependencies of the separation regimes are not addressed in the model, an important issue for droplets in high-temperature gases.

A series of molecular dynamics (MD) simulations was performed to determine the effects of small droplet sizes and variable droplet temperatures on the coalescence model.[34] Collisions of two nano-sized droplets each containing 2500 molecules at various impact parameters and Weber numbers were simulated using the computational tool of Micci et al.[35] We assume that the physics of the collisions between nano-sized and micron-sized particles are similar. Simulations were run for Weber numbers of 10, 15, 20, 25, and

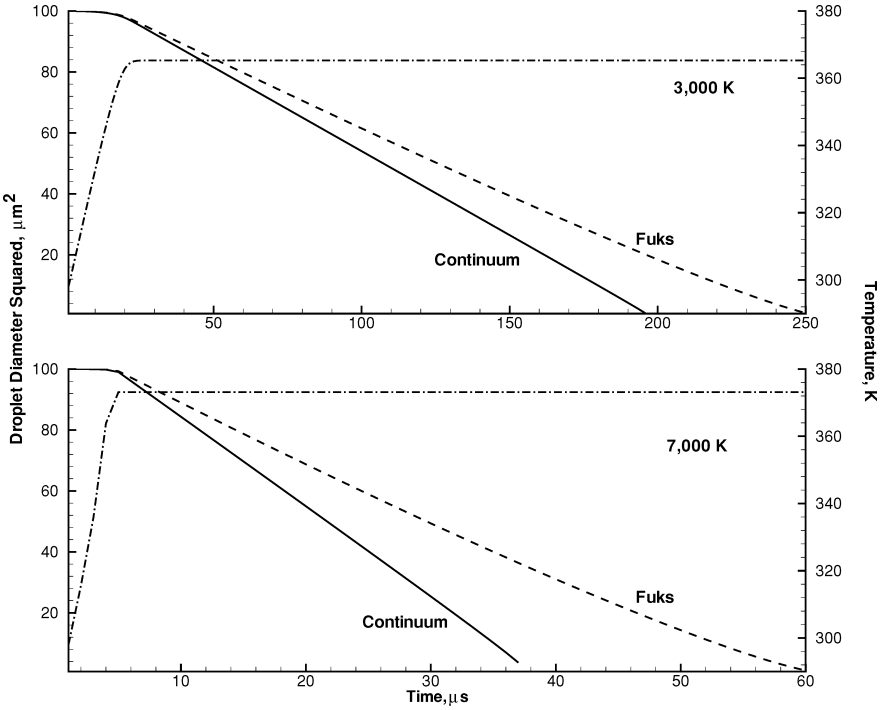

Fig. 4 Droplet temperature and diameter profiles for 10-μm droplets in a 3000 and 7000-K environment. Dashed lines indicate the square of the droplet diameter for the full, corrected continuum model. Solid lines indicate behavior corresponding to the d^2 continuum law; that is, without rarefied gas effects. The droplet temperature curves are indicated by the dot-dashed line.

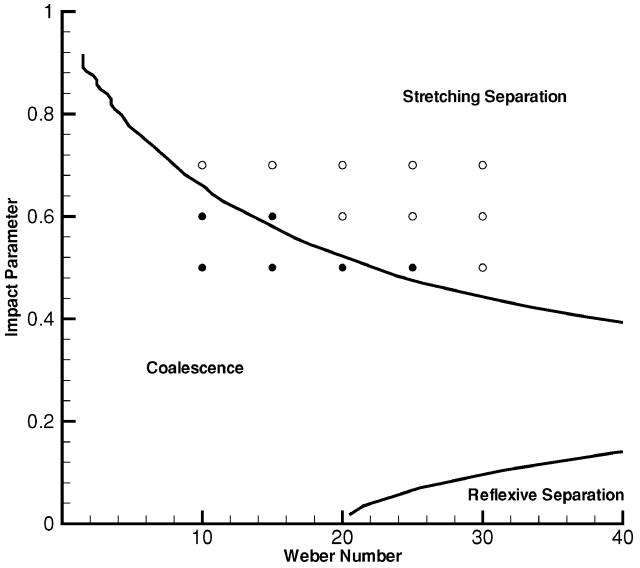

Fig. 5 Regimes of coalescence and separation based on the Ashgriz–Poo model for a droplet size ratio of 1.0. Open circles represent stretching separation and closed circles represent coalescence as determined with MD simulations (adapted from Ref. 6 with permission).

30; droplet temperatures of 300, 320, 340, and 360 K; and impact parameters of 0.5, 0.6, and 0.7. We have used a Lennard–Jones (12,6) potential with a well depth of 761.7 K and zero potential point at 0.274 nm, calculated from the critical temperature of water.[36] Results of MD simulation are shown in the inset of Fig. 5, where open circles represent a simulation outcome of stretching separation and closed circles represent coalescence.

The MD simulations were able to resolve collisions within the separation regime consistent with the predictions of the Ashgriz and Poo model.[33] In addition, the boundary between separation and coalescence was unchanged over the range of droplet temperatures (298–373 K) studied. Thus, the coalescence model of Ashgriz and Poo[33] is implemented in the DSMC aerosol simulation with no modification.

The implementation of the coalescence procedure in the DSMC modeling consists of two parts: droplet-pair selection and evaluation of the droplet collision outcome. The droplets were considered to be spherically symmetric rigid spheres in the procedure of droplet–droplet collisions, and the hard-sphere model was used to calculate the collision frequency. The majorant frequency scheme was used to model the collision procedure, with actual collisions selected based on the droplet relative collision velocity and the hard-sphere total collision cross section.[11] The change of the hard-sphere collision cross section due to droplet evaporation or coalescence was accounted for in the simulations. If a droplet pair is selected for a collision, the outcome is then calculated based on the coalescence probability calculated for the given pair. A coalescence outcome is determined using the Ashgriz and Poo[33] model as discussed earlier. The collisional Weber number and droplet size ratio are calculated from the droplet diameters and the relative droplet–droplet velocity, while the impact parameter is stochastically determined using the inverse-cumulative method.[7] Upon coalescence, one of the droplets is removed from the simulation domain and the mass of the other droplet is increased accordingly. The droplet diameter is recalculated from the new droplet mass. In addition, the temperature of the new droplet is determined from the thermal masses of the two initial droplets. Assuming conservation of momentum, the axial and radial velocities of the new droplet are recalculated. If the collision leads to separation, the droplets are preserved with new calculated velocities. Mass transfer from one droplet to the next is negligible because the time interval between coalescence and separation is short for micrometer-sized droplets. The range of coalescence probability values predicted by the model of Ashgriz and Poo is between 0.2 and 1 for the cases considered here. The reflexive separation process is fully resolved in the DSMC simulations, although it is unlikely due to the low kinetic energies of collision for the conditions of interest.

VI. Results and Discussion

We now present results of two general classes of simulation. First we consider the hypothetical case of a spatially uniform background-gas temperature with initial particle conditions of a single diameter and a particle velocity distribution corresponding to that of a DIHEN device (bottom two portions of Fig. 6). The background gas is assumed to be stagnant and the pressure is 1 atm. The second case that will be examined is that of a spatially variable background-gas temperature and velocity corresponding to the ICP with the particle diameter, number flux, and velocity distributions shown in Fig. 6. For both cases, the axisymmetric SMILE computational tool was used in the simulations.

The DSMC simulation domain typically consists of 12,000 cells and extends 50 mm axially and 9 mm radially. The droplets are introduced from the left boundary into the simulation domain with a jet of radius 0.75 mm, and an average steady state of 75,000 droplets are simulated for a minimum of 100,000 time steps. A time step of 10^{-7}–10^{-6} s was used, with the smaller value used in the simulation of 1-μm droplets.

Figures 7 and 8 show the predicted number and mass density, respectively, of a spray of monosized 10-μm droplets in a uniform 2000-K background gas. The figures show the predictions of the full model (top portions of Figs. 7 and 8), and results without coalescence (middle portions of Figs. 7 and 8) and without the use of mass transfer corrections (bottom portions of Figs. 7 and 8). For the last case (bottom portions of Figs. 7 and 8), the removal of the Fuks corrections means that the continuum model for droplet evaporation is assumed; however, particle coalescence is also included. When coalescence is included in the simulation, the number density of droplets decreases rapidly from the droplet injection point, indicating that coalescence is an important loss process.

The figures show that the inclusion of coalescence is important to the final number and mass density of droplets, allowing the aerosol to penetrate the simulation domain to a distance four to five times greater than when coalescence is not included. The middle portions of Figs. 7 and 8 show that when coalescence is ignored the droplets are stopped by the stagnant background gas and a region

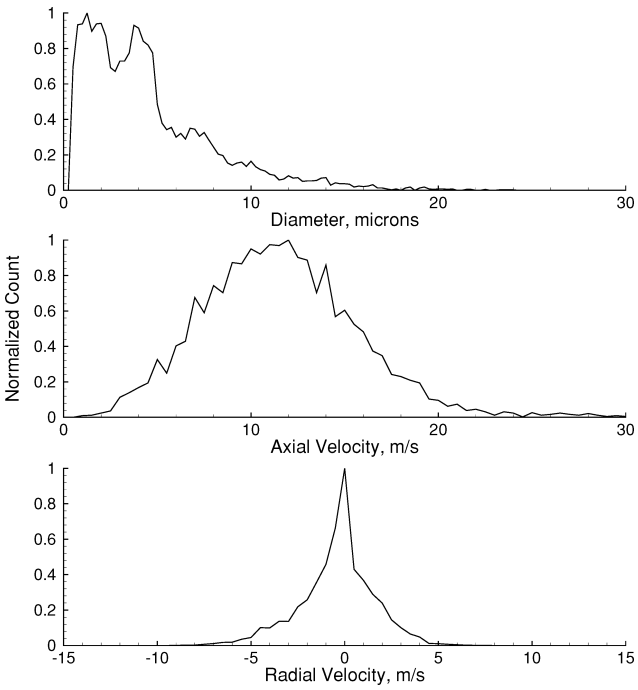

Fig. 6 DIHEN initial droplet sizes and velocities assumed in the calculations. (Data are taken from the phase-Doppler particle analyzer measurements of McLean et al.[8] with permission.)

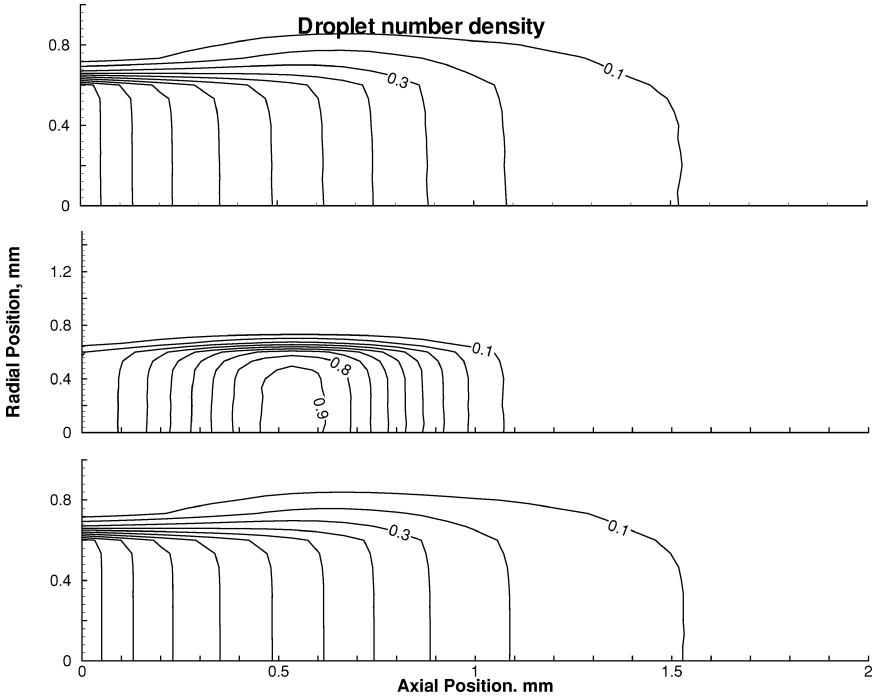

Fig. 7 Normalized number density of aerosol for a monosize distribution of 10-μm droplets in a 2000-K gas. Top figure indicates inclusion of heating, desolvation, transport, and coalescence, with all rarefied gas effects included. The middle figure neglects the effects of coalescence, while the bottom figure assumes continuum evaporation models and coalescence. Top and bottom figures are normalized to 4.0×10^{13} droplets/m^3; middle figure is normalized to 4.0×10^{14} droplets/m^3.

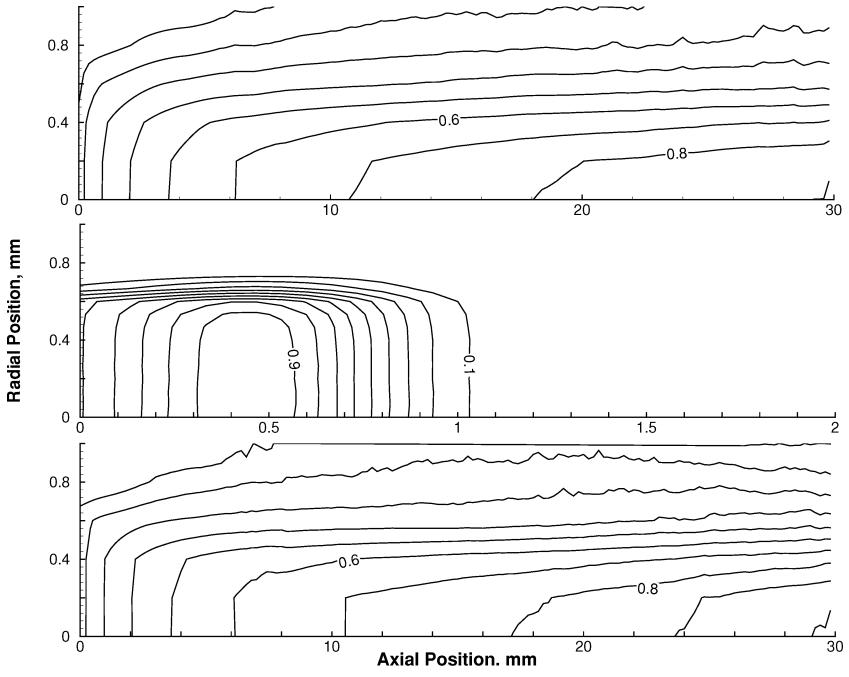

Fig. 8 Normalized mass density of aerosol for a monosize distribution of 10-μm droplets in a 2000-K gas. The top simulation includes droplet heating, desolvation, transport, and coalescence, with all rarefied gas effects. The middle simulation plot neglects the effects of coalescence, while the bottom simulation plot assumes continuum evaporation models and coalescence. Top and bottom figures are normalized to 180 kg/m^3; middle figure is normalized to 75 kg/m^3.

of droplet "accumulation" is formed. For the conditions of initially sized 10-μm droplets at 2000 K, the inclusion of the Fuks correction does not change the spatial distribution of the aerosols in the flow. These results are due to the relatively large initial size of the aerosol droplets.

Figure 9 shows the ratio of the droplet number density calculated without coalescence to the number density calculated with coalescence. Results are shown for 10-μm droplets in 300-, 1000-, and 2000-K gases. Because coalescence causes a reduction in number density, the number density calculated without coalescence is higher at the inflow boundary. However, the droplets soon come to an accumulation region (see the middle portions of Figs. 7 and 8), which is represented by maxima in the number density ratio curves, and subsequently evaporate. At further axial depths, the droplet number density with coalescence may exceed that calculated without coalescence, as can be seen in the slight rise of the 2000-K curve for axial

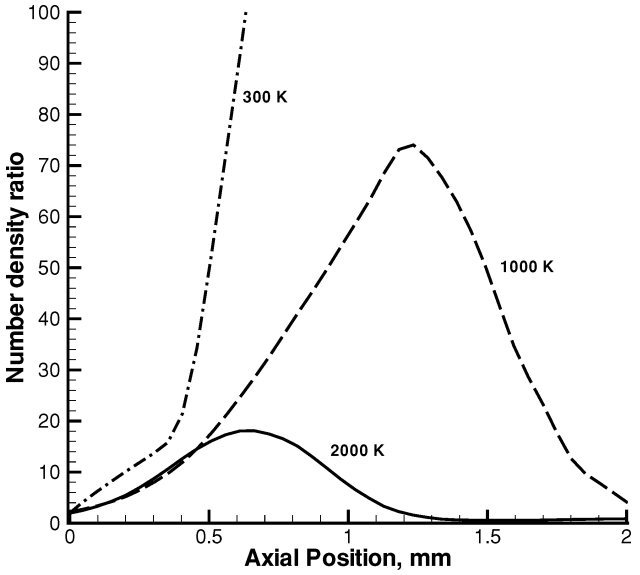

Fig. 9 Ratio of droplet number density along the axial direction for 10-μm droplets without and with coalescence for different background-gas temperatures.

distances greater than approximately 1.4 mm. As the gas temperature becomes lower, the coefficient of viscosity decreases thereby decreasing the drag force so that droplets can proceed through the simulation domain to greater axial depths. The lower background-gas temperatures also increase the length of droplet evaporation time, thus causing the number density ratio to be much higher.

The effect of gas temperature on the mass density of 10-μm droplets can be further illustrated by Fig. 10 for the full model. Figure 10 shows mass density contour plots and trends along the axial axis for 10-μm droplets at background-gas temperatures of 300, 1000, and 2000 K. At 300 K, a droplet accumulation region exists at a depth between 10 and 15 mm into the simulation domain. An increase in temperature causes the accumulation region to appear at increased axial depths despite the higher desolvation rate. The mass density increases at a higher rate at increased gas temperatures, as illustrated in the bottom portion of Fig. 10, because of a stronger drag force resulting from a higher gas viscosity.

To illustrate the effect of droplet size, Fig. 11 presents the normalized mass density and Fig. 12 the normalized number density of 1-μm droplets in a 1000-K gas. All curves in Fig. 11 are normalized to 0.017 kg/m^3, while the curves in Fig. 12 are normalized to 1.0×10^{15} droplets/m^3. Again, the top field in each figure represents results obtained with the full aerosol model, the middle field neglects the effects of coalescence, and the bottom field neglects the Fuks mass transfer correction. All evaporation occurs within a very short distance of the droplet injection point. Note that a region of droplet accumulation exists just beyond 0.01 mm into the simulation. The drag force causes rapid deceleration for small droplet sizes, prohibiting further penetration into the simulation domain.

As can be seen by the top and center contours of both plots, coalescence has a negligible effect on the droplet number and mass densities of 1-μm droplets moving in a static, background gas at 1000 K. The collision cross section of 1-μm droplets is sufficiently small such that coalescence events are rare even in the droplet accumulation region. However, the Fuks correction extends the time that droplets remain in the simulation, causing an increase in the droplet number density. The maximum droplet mass density, when the Fuks correction is not utilized, is approximately half of the maximum droplet number density when it is used. In addition, note that the accumulation region lies further into the simulation domain when the Fuks correction is used. Because the droplets maintain a larger size for longer periods of time, Stokes's law has a lesser effect on the droplets, allowing a slight increase in droplet penetration.

Figures 13 and 14 represent the mass density (normalized to 0.08 kg/m^3) and the number density (normalized to 5.0×10^{14}

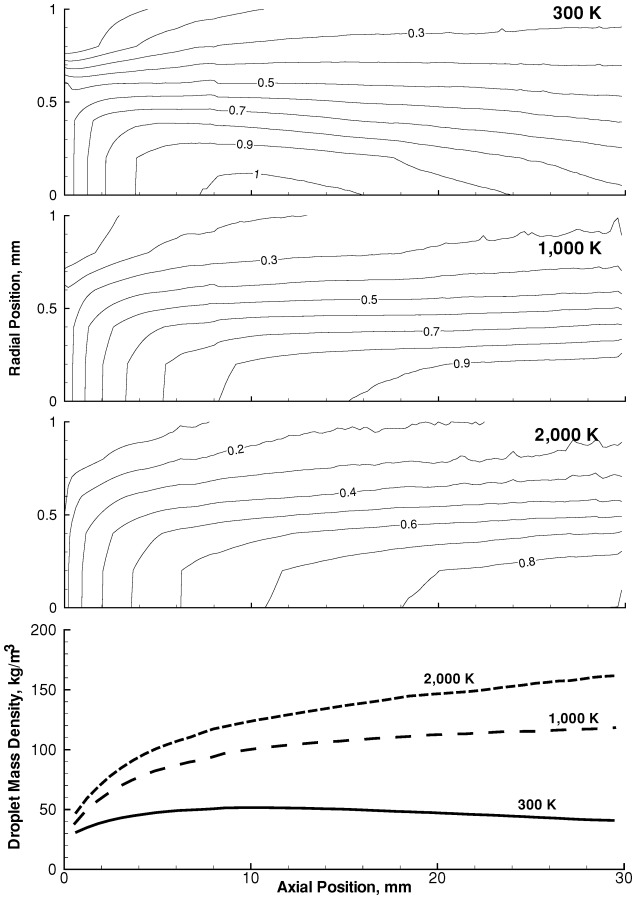

Fig. 10 Mass density contour plots of 10-μm droplets at background-gas temperatures of 300, 1000, and 2000 K. The normalization factors for the three contour plots are 50.0, 120.0, and 180.0 kg/m^3 for temperatures of 300, 1000, and 2000 K, respectively. The bottom figure shows the mass density along the axial axis for the three different background-gas temperatures.

droplets/m^3), respectively, of 1-μm droplets in a 2000-K gas. Again, the top field represents results obtained using the full aerosol model, the center field neglects the effects of droplet coalescence, and the bottom field neglects the Fuks mass transfer correction. As was noted previously, coalescence has a negligible effect on the behavior of 1-μm droplets due to their small collision cross sections. In addition, the Fuks mass transfer correction is much more influential than in the 1000-K-gas case, causing a reduction in the maximum mass density by approximately a factor of 3. Note that droplet penetration into the simulation domain is reduced compared to 1-μm droplets in a 1000-K gas. The gas viscosity increases with temperature, causing drag to have a greater influence on the droplet velocity. Thus, droplets in a 2000-K gas move more slowly and do not progress into the simulation domain to as great an extent. While the Cunningham slip-flow correction factor partially counteracts this trend due to the higher mean free path of the 2000-K gas, the axial position of the 0.1 mass density contour is reduced by approximately 30%.

To demonstrate the applicability of the aforementioned model to a more complex system, the resultant spatial distribution of particle sizes and mass density from a liquid aerosol ejected from a DIHEN[8] into an Ar ICP is simulated. The nebulizer chosen for this study is the DIHEN, a micronebulizer for applications in which sample is limited, expensive, or toxic.[8] The DIHEN is typically operated at a gas flow and a solution uptake rate of 0.2 liter/min and 85 μl/min, respectively, leading to a Sauter mean diameter (the droplet volume-to-surface-area ratio) of 10.11 μm.[8] The specific initial droplet size distribution used in these simulations is given in Fig. 6. Argon temperatures, number densities, and velocities are generated by the high-frequency induction plasma (HiFI) code.[37,38] The HiFI code solves the Navier–Stokes equations with the SIMPLER algorithm

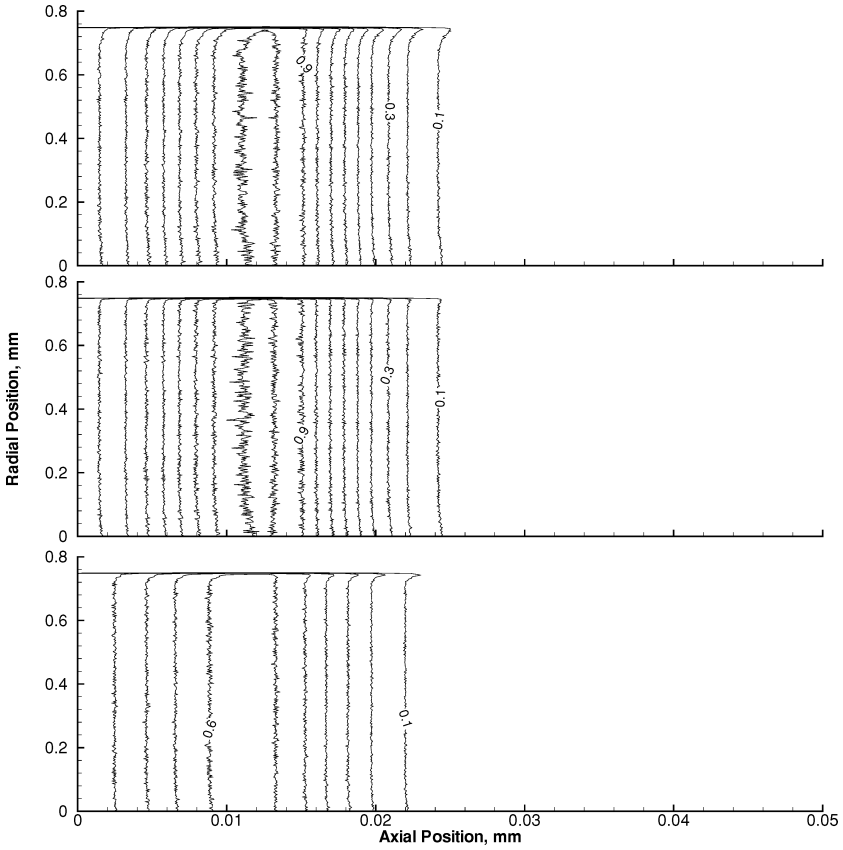

Fig. 11 Normalized mass density contour plots (normalized to 0.017 kg/m^3) of 1-μm droplets at a background-gas temperature of 1000 K. The top figure indicates inclusion of heating, desolvation, transport, and coalescence, with all rarefied gas effects included. The middle figure neglects the effects of coalescence, and the bottom figure assumes continuum evaporation models and coalescence.

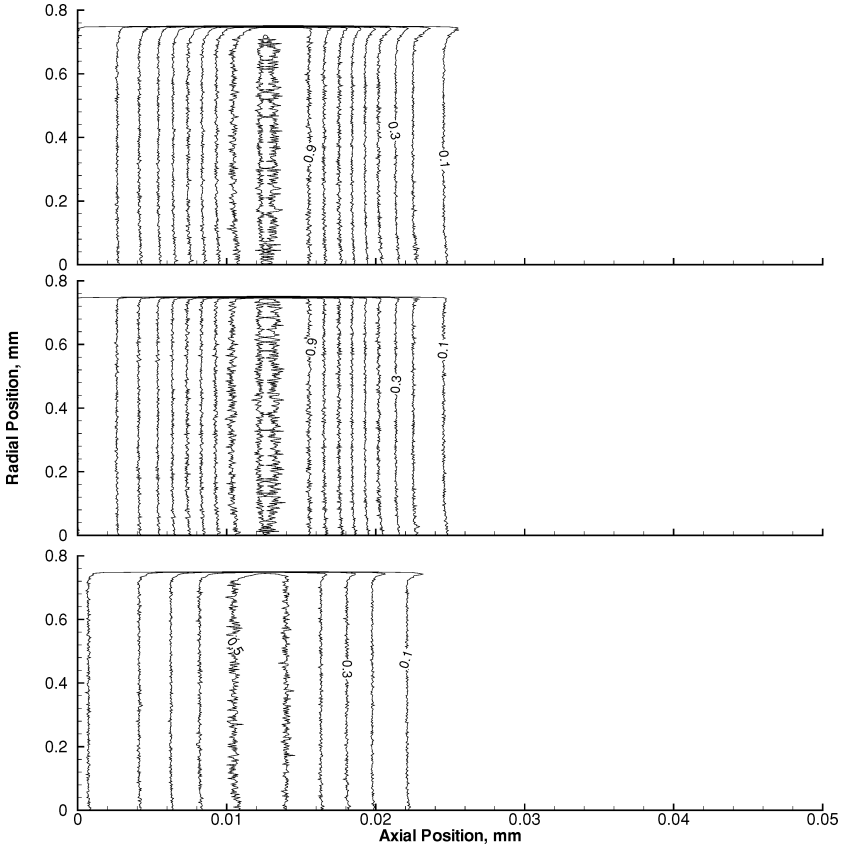

Fig. 12 Normalized number density contour plots (normalized to 1.0×10^{15} droplets/m^3) of 1-μm droplets at a background-gas temperature of 1000 K. The top figure indicates inclusion of heating, desolvation, transport, and coalescence, with all rarefied gas effects included; The middle figure neglects the effects of coalescence; and the bottom figure assumes continuum evaporation models and coalescence.

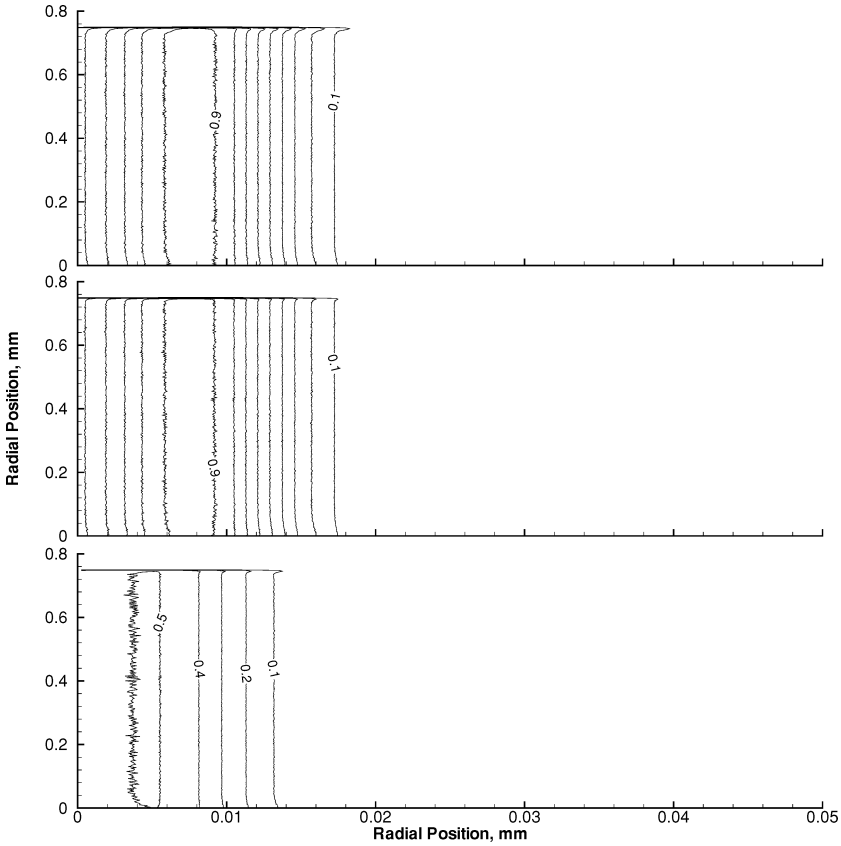

Fig. 13 Normalized mass density contour plots (normalized to 0.080 kg/m^3) of 1-μm droplets at a background-gas temperature of 2000 K. The top figure indicates inclusion of heating, desolvation, transport, and coalescence, with all rarefied gas effects included; the middle figure neglects the effects of coalescence; and the bottom figure assumes the use of the continuum evaporation models and coalescence.

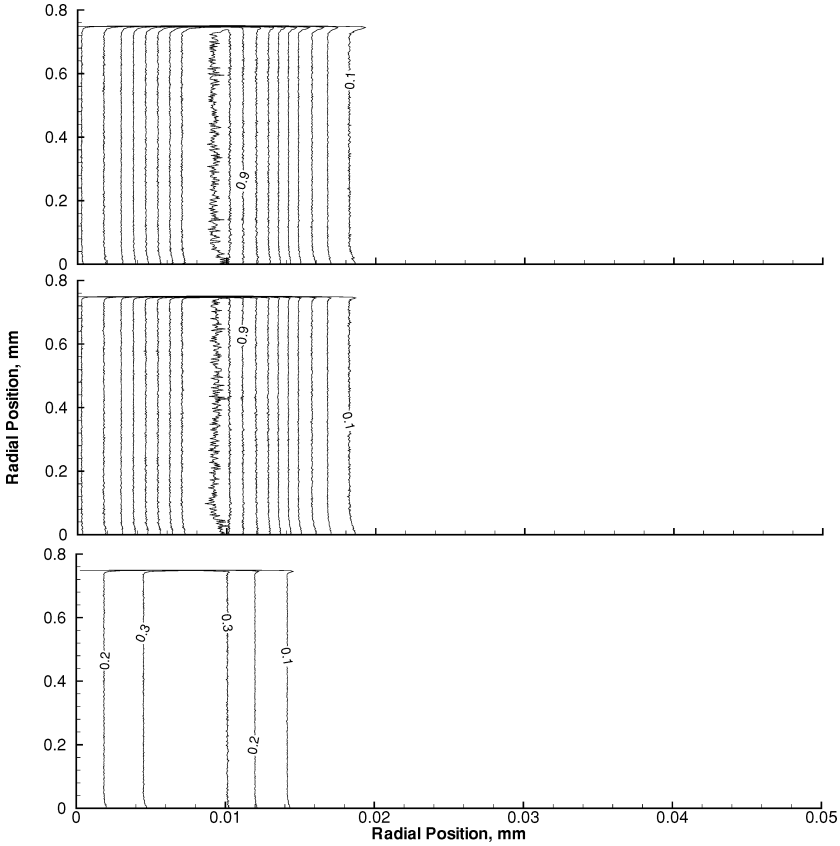

Fig. 14 Normalized number density contour plots (normalized to 5.0 $\times$ 10^{14} droplets/m^3) of 1-μm droplets at a background-gas temperature of 2000 K. The top figure indicates inclusion of heating, desolvation, transport, and coalescence, with all rarefied gas effects included; the middle figure neglects the effects of coalescence; and the bottom figure assumes the use of the continuum evaporation models and coalescence.

to determine key fundamental properties of the ICP. Predicted gas temperatures range from 3000 K along the axial channel and in outlying regions to greater than 10,000 K in the hottest portions of the plasma.[37] The temperature contours predicted for a 1500-W Ar ICP by the HiFI code are shown in Fig. 15.

The numerical parameters for the nebulizer simulations are as follows. The radius enclosed by the simulation is 4.0 mm from the center of the plasma and extends to a depth of 3.0 cm within the plasma. Although HiFI predicts temperatures and number densities for a plasma approximately 5 cm long with a radius of 1 cm, all droplet evaporation occurs within the smaller computational domain and, thus, any extension of the simulation beyond that point is unnecessary. Other numerical parameters such as the computational grid and time step are similar to those used in the earlier results.

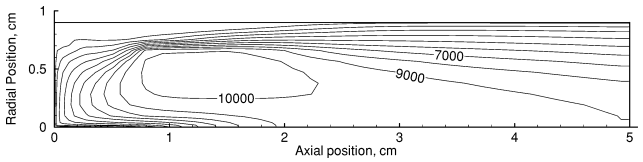

Fig. 15 Temperature contours typical of the Ar ICP, as predicted in this work with the HiFI code. Argon gas temperatures can reach 10,000 K in the induction region of the plasma and remain at 3000–5000 K within the center and outlying regions. The plasma is assumed to be axisymmetric, with the symmetry axis at $y = 0$. Droplets are injected from the bottom left of the figure.

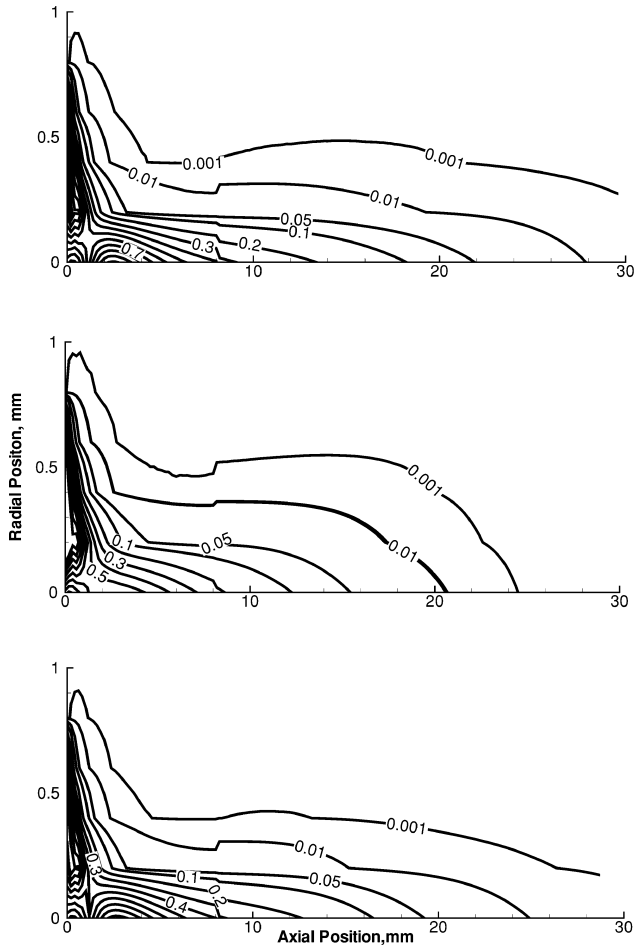

Fig. 16 Predictions of DIHEN droplet mass density contours. The top figure indicates inclusion of heating, desolvation, transport, and coalescence, with all rarefied gas effects included; the middle figure neglects the effects of coalescence; and the bottom figure assumes the use of the continuum evaporation model and coalescence throughout the simulation. The top and bottom figure contours are normalized by 12 kg/m^3, and the middle set of contours is normalized by 8 kg/m^3.

The computed spatial distribution of DIHEN droplet mass density in an Ar ICP is shown in Fig. 16. As in earlier figures, simulations are shown for the full model (top), calculations that neglect coalescence (middle), and a model that assumes the use of continuum evaporation and coalescence (bottom). Note that the aerosol distribution is stretched along the axial channel due to lower gas temperatures and higher gas velocities. Again, note that the computational domain is smaller than the full HiFI domain shown in Fig. 15. The simulation shown in the top portion of Fig. 16 indicates that 10% by mass of the aerosol (defined as the sum of the masses of all droplets within the simulation) is present at distances up to 19.0 mm from the beginning of the plasma. Results without coalescence (middle portion of Fig. 16), suggest that the boundary of the 10% of aerosol mass lies 11.0 mm into the simulation domain.[3] Similar trends among the three models were also observed for the 1% droplet mass contours. Thus, the inclusion of coalescence in the simulation significantly increases the effective lifetime of the droplets in the plasma. Note also that the Fuks mass transfer correction primarily impacts small droplets. Thus, it significantly changes the number density but has relatively little influence on the final mass density of aerosol.

VII. Conclusions

A computer model has been constructed to determine the spatial distribution of liquid aerosols in high-temperature gas environments. The model is based on a DSMC particle-simulation technique that enables the inclusion of important droplet rarefaction effects; yet, it is sufficiently general such that the entire two-phase flow system can be simulated. Due to finite Knudsen number correction factors applied to the mass transfer and transport portions of the code, the model is valid at high gas temperatures, low gas pressures, or for small droplets, offering a wide range of conditions for which the model is applicable.

Different modeling options were considered for the key four aspects of the computational tool: droplet heating, desolvation, transport, and coalescence. The results showed that the Fuks corrections should be used to model droplet heating and desolvation. Comparison of exact single-sphere DSMC simulations of the drag force against a sphere with different analytic slip-flow models shows that the Cunningham correction applied to the Stokes law gives the best model for droplet transport. The Ashgriz–Poo model for droplet coalescence, one of the most important of the processes, was chosen based on comparisons with fundamental MD simulations. These comparisons showed that the outcome of droplet–droplet collisions does not appear to have a temperature dependence over the range tested. The four aforementioned selections represent the baseline model recommended for the two-phase flow conditions considered here.

The computational tool was applied to two general classes of simulation results. A spatially uniform background-gas temperature with a particle velocity distribution and a spatially variable background-gas distribution corresponding to that of an ICP were considered. The key results for the uniform background gas are as follows. As droplet size increases, the coalescence process increases in importance. For 1-μm particles in a background gas of temperatures in the 1000–2000-K range, the Knudsen number is sufficiently large that the use of the continuum evaporation model leads to incorrect droplet evaporation rates. The simulation was also applied to the case of nebulizer droplets from a DIHEN introduced into an ICP. It was found that inclusion of both coalescence and noncontinuum gas effects is also crucial to the modeling of this more complex spray system.

Acknowledgments

This research was sponsored by the U.S. Army Awards for Science and Engineering Research Training (ASSERT) Program under Grant DAAG55-98-1-0209 and the U.S. Department of Energy under Grant DE-FG02-93ER14320. Additional support was provided for S. Gimelshein, J. Zhong, and D. Levin under U.S. Army Research Office Grant DAAG55-98-1-0236. Thanks are due to M. Ivanov of the Institute of Theoretical and Applied Mechanics, Russia, for use of the SMILE code. We are grateful to J. Mostaghimi (University

of Toronto, Canada) for providing the HiFI code and to Michael M. Micci for the use of his molecular dynamics code and for several discussions.

References

[1]Clampitt, N. C., and Hieftje, G. M., "Investigation into the Mechanism of Desolvation of Sample Droplets in Flame Spectrometry," *Analytical Chemistry*, Vol. 44, No. 7, 1972, pp. 1211–1219.

[2]Horner, J. A., Lehn, S. A., and Hieftje, G. M., "Computerized Simulation of Aerosol-Droplet Desolvation in an Inductively Coupled Plasma," *Spectrochimica Acta, Part B: Atomic Spectroscopy*, Vol. 57, 2002, pp. 1025–1042.

[3]Benson, C. M., Gimelshein, S. F., Levin, D. A., and Montaser, A., "Simulation of Droplet Heating and Desolvation in an Inductively Coupled Plasma—Part I," *Spectrochimica Acta Part B: Atomic Spectroscopy*, Vol. 56, 2001, pp. 1097–1112.

[4]Benson, C. M., Gimelshein, S. F., Levin, D. A., and Montaser, A., "Simulation of Droplet-Gas Interactions in an Inductively Coupled Plasma Using the Direct Simulation Monte Carlo Method," AIAA Paper 2000-2431, June 2000.

[5]Benson, C. M., Gimelshein, S. F., Levin, D. A., and Montaser, A., "Modeling of Droplet Evaporation and Coalescence for Direct Injection into an Inductively Coupled Plasma," AIAA Paper 2001-3037, June 2001.

[6]Benson, C. M., Gimelshein, S. F., Levin, D. A., and Montaser, A., "Simulation of Droplet Heating and Desolvation in an Inductively Coupled Plasma—Part II: Coalescence in the Plasma," *Spectrochimica Acta, Part B: Atomic Spectroscopy*, Vol. 58, No. 8, 2003, pp. 1453–1471.

[7]Bird, G. A., *Molecular Gas Dynamics and the Direct Simulation of Gas Flows*, Clarendon, Oxford, 1994.

[8]McLean, J. A., Zhang, H., and Montaser, A., "A Direct Injection High-Efficiency Nebulizer for Inductively Coupled Plasma Mass Spectrometry," *Analytical Chemistry*, Vol. 70, No. 5, 1998, pp. 1012–1020.

[9]Montaser, A. (ed.), *Inductively Coupled Plasma Mass Spectrometry,* Wiley-VCH, New York, 1998.

[10]Montaser, A., and Golightly, D. W. (eds.), *Inductively Coupled Plasmas in Analytical Atomic Spectrometry*, 2nd ed., Wiley-VCH, New York, 1992.

[11]Ivanov, M. S., and Rogasinsky, S. V., "Analysis of Numerical Techniques of the Direct Simulation Monte Carlo Method in the Rarefied Gas Dynamics," *Soviet Journal of Numerical Analysis and Mathematical Modeling,* Vol. 2, 1988, pp. 453–465.

[12]Vincenti, V. C., and Kruger, C. H., *Introduction to Physical Gas Dynamics*, Wiley, New York, 1965.

[13]Ivanov, M. S., Markelov, G. N., and Gimelshein, S. F., "Statistical Simulation of Reactive Rarified Flows: Numerical Approach and Applications," AIAA Paper 98-2669, June 1998.

[14]Cunningham, E., "On the Velocity of Steady Fall of Spherical Particles through Fluid Medium," *Proceedings of the Royal Society of London. Series A: Mathematical and Physical Sciences*, Vol. 83, 1910, pp. 357–365.

[15]Stalder, J. R., and Zurick, V. J., "Theoretical Aerodynamic Characteristics of Bodies in a Free-Molecular-Flow Field," NACA TN 2423, July 1951.

[16]Tsien, H.-S., "Superaerodynamics, Mechanics of Rarefied Gases," *Journal of Aerosol Science*, Vol. 13, 1946, pp. 653–664.

[17]Larin, M., Lumpkin, F., and Stuart, P., "Modeling Unburned Propellant Droplet Distribution and Velocities in Plumes of Small Bipropellant Thrusters," AIAA Paper 2001-2816, June 2001.

[18]Phillips, W. F., "Drag on a Small Sphere Moving Through a Gas," *Physics of Fluids*, Vol. 18, No. 9, 1975, pp. 1089–1093.

[19]Hinds, W. C., *Aerosol Technology: Properties, Behavior, and Measurement of Airborne Particles*, Wiley, New York, 1982.

[20]Chin, J. S., and Lefebvre, A. H., "The Role of the Heat-Up Period in Fuel Drop Evaporation," *International Journal of Turbo and Jet Engines*, Vol. 2, 1985, pp. 315–325.

[21]Lefebvre, A. H., *Atomization and Sprays*, Hemisphere, New York, 1989.

[22]Aref'Yev, K. M., and Averkiyev, A. G., "Physics of Heat and Mass Transfer During Evaporative Cooling of Water," *Heat Transfer—Soviet Research,* Vol. 11, No. 5, 1979, pp. 135–142.

[23]Carey, V. P., Oyumi, S. M., and Ahmed, S., "Post-Nucleation Growth of Water Microdroplets in Supersaturated Gas Mixtures: A Molecular Simulation Study," *International Journal of Heat and Mass Transfer*, Vol. 40, No. 10, 1997, pp. 2393–2406.

[24]Hubbard, G. L., Denny, V. E., and Mills, A. F., "Droplet Evaporation: Effects of Transients and Variable Properties," *International Journal of Heat and Mass Transfer*, Vol. 18, No. 9, 1975, pp. 1003–1008.

[25]Sparrow, E. M., and Gregg, J. L., "The Variable Fluid-Property Problem in Free Convection," *Transactions of the American Society of Mechanical Engineers*, Vol. 80, 1958, pp. 879–886.

[26]Young, J. B., "The Condensation and Evaporation of Liquid Droplets at Arbitrary Knudsen Number in the Presence of an Inert Gas," *International Journal of Heat and Mass Transfer*, Vol. 36, No. 11, 1993, pp. 2941–2956.

[27]Fuks, N. A., "On the Stationary Charge Distribution on Aerosol Particles in a Bipolar Ionic Atmosphere," *Geofisica Pura e Applicata*, Vol. 56, 1963, pp. 185–193.

[28]Fuks, N. A., "On the Theory of the Evaporation of Small Droplets," *Soviet Physics—Technical Physics*, Vol. 3, 1958, pp. 140–143.

[29]Filippov, A. V., and Rosner, D. E., "Energy Transfer Between an Aerosol Particle and Gas at High Temperature Ratios in the Knudsen Transition Regime," *International Journal of Heat and Mass Transfer*, Vol. 43, 2000, pp. 127–138.

[30]Willis, K. D., and Orme, M. E., "Experiments on the Dynamics of Droplet Collisions in a Vacuum," *Experiments in Fluids*, Vol. 29, No. 4, 2000, pp. 347–358.

[31]Qian, J., and Law, C. K., "Regimes of Coalescence and Separation in Droplet Collision," *Journal of Fluid Mechanics,* Vol. 331, 1997, pp. 59–80.

[32]Orme, M., "Experiments on Droplet Collisions, Bounce, Coalescence and Disruption," *Progress in Energy and Combustion Science*, Vol. 23, 1997, pp. 65–79.

[33]Ashgriz, N., and Poo, J. Y., "Coalescence and Separation in Binary Collisions of Liquid Drops," *Journal of Fluid Mechanics*, Vol. 221, 1990, pp. 183–204.

[34]Benson, C. M., "An Advanced Model for the Determination of Aerosol Droplet Lifetime in an Inductively Coupled Plasma," Ph.D. Dissertation, Dept. of Chemistry, George Washington University, Washington, DC, 2002.

[35]Micci, M. M., Kaltz, T. L., and Long, L. N., "Molecular Dynamics Simulations of Atomization and Spray Phenomena," *Atomization and Sprays*, Vol. 11, 2001, pp. 351–363.

[36]Gotoh, K., "Liquid Structure and Lennard-Jones (6,12) Pair Potential Parameters," *Nature: Physical Science*, Vol. 239, No. 96, 1972, pp. 154–156.

[37]Mostaghimi, J., Proulx, P., and Boulos, M. I., "An Analysis of the Computer Modeling of the Flow and Temperature Fields in an Inductively Coupled Plasma," *Numerical Heat Transfer*, Vol. 8, No. 2, 1985, pp. 187–201.

[38]Cai, M., Haydar, D. A., Montaser, A., and Mostaghimi, J., "Computer Simulation of Argon-Nitrogen and Argon-Oxygen Inductively Coupled Plasmas," *Spectrochimica Acta Part B: Atomic Spectroscopy*, Vol. 52, 1997, pp. 369–386.